Static and Dynamic Loads on a Shallow Circular Tunnel: Practical Design Considerations

L. Medina[1]([envelope]) [ORCID], C. Gutiérrez[1] [ORCID], B. Lyon[1] [ORCID], and G. Candia[2] [ORCID]

[1] Faculty of Civil Engineering, Universidad del Desarrollo, Santiago, Chile
`lumedinam@udd.cl`
[2] Faculty of Civil Engineering, Santiago-Chile, and National Research Center for Integrated Natural Disaster Management (CIGIDEN), ANID/FONDAP/15110017, Universidad del Desarrollo, Santiago, Chile

Abstract. In the current study we analyze the lining forces developed on a shallow circular tunnel in medium sand under two loading conditions: (i) gravity loads, and (ii) static plus dynamic loads due to ground motions. Motivated by the field performance of actual tunnels, the purpose of this study is to explore a recurrent question regarding the safety of tunnels and other underground facilities: "does a shallow tunnel properly designed to resist static loads has enough safety margins to withstand severe ground shakings without significant damage?".

The study unit is a typical 0.3 m thick sprayed concrete tunnel, 6 m in diameter, and built in a 60 m deep deposit of Leighton Buzzard sand (Dr 75%) at a crown depth of 12 m. The soil deposit has a total width of 140 m, free field boundary conditions, and is underlain by an elastic halfspace with a shear wave velocity of 760 m/s. A 2D plain strain finite element model was implemented in OpenSees [1]. The tunnel was modeled using elastic frame elements and the soil's stress-strain behavior was modeled using the PressureDepenMultiYield [2] constitutive relation. A quiet (absorbing) boundary was added at the model base to dissipate the rebounding shear waves [3].

After the initial gravity analysis of a uniform soil deposit, the static lining forces were obtained from a 4-staged excavation analysis, in which one quarter of the circle was removed and the corresponding lining elements were added at each stage. To characterize the dynamic loads on the tunnel, and properly account for the ground motion variability, a set of 112 records from subduction interface earthquakes [4] were used to run non-linear time history analyses. Our results suggest that tunnels designed statically can indeed undergo significant shaking without excessive damage.

Keywords: tunnels · seismic design · finite elements

1 Introduction

Metro tunnels are a critical component of the transportation network in major cities worldwide. In active seismic environments, these systems can be severely damaged during an earthquake due to ground failure or ground deformations, leading to a loss of

functionality of the network, significant economic losses, and social consequences. In absence of ground failure, and despite the good seismic performance of shallow tunnels in recent events (e.g., the 2010 Maule earthquake or 2011 Tohoku earthquake), experimental evidence shows that tunnels can suffer large deformations due dynamic soil-structure interaction. Indeed, available centrifuge models capture this kinematic and inertial interaction reasonably well, yet the focus is not placed on modeling the structural damage, which is an important limitation.

An appealing explanation for the limited damage observed in concrete tunnels is the overdesign implicit in current design codes. Thus, in the present study, we compare the margins of safety on a tunnel designed statically, i.e., without seismic considerations, for two loading conditions: (1) static or gravity loads, which accounts for the excavation and construction sequence, and (2) static plus dynamic loads. A finite element model of the soil and tunnel were implemented and a ground motion set is defined consistent with the hazard levels for a tunnel located hypothetically in Santiago.

2   Numerical Modelling

A plain strain finite element model of the tunnel and soil deposit was implemented in OpenSees; it consists of a medium-density Leighton Buzzard sand (LBS) deposit 140 m wide and 60 m deep, and a circular tunnel modeled with linear elements, 6 m diameter, located 12 m below the ground surface (see Fig. 1). For simplicity, the tunnel interior (i.e., soil to be excavated) was discretized with triangular elements, while a regular mesh of four-node elements was used elsewhere.

To simulate free field conditions, two soil columns 15 m wide were added at the model boundaries. These columns are constrained to have equal displacements at nodes located at the same depth. Additionally, an array of bidirectional viscous dampers is added at the base, which allows dissipating the waves reflected on the free surface and the waves scattered by the presence of the lining (Lyon et al. 2022).
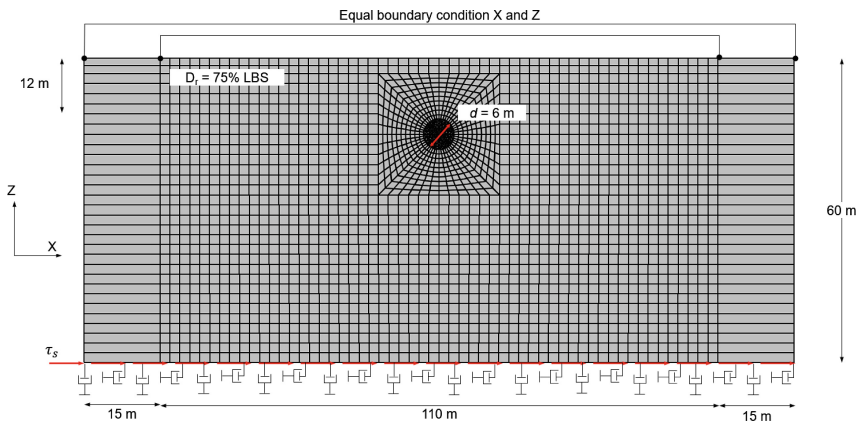

Fig. 1. Mesh of the finite element model (2D) of the soil-tunnel system.

The stress-strain relationship for Leighton Buzzard Sand (LBS) was modeled with the PressureDependMultiYield material (PDMY, Yang & Elgamal 2003) available on OpenSees. This material allows simulating the hysteretic response of sands and silts whose stiffness and strength is a function of the confining pressure. A salient feature of PDMY is its ability to simulate arbitrary stress paths, volumetric changes induced by shear (or dilatancy), and liquefaction. The PDMY parameters used in the present study are summarized in Table 1; these parameters are derived from a 3-stage calibration analysis by Lyon et al. (2022), which accounts for: (1) the simulation of a soil-tunnel seismic response and validation against centrifuge data, (2) the simulation of a 1D soil column under seismic loading and comparison against a linear-equivalent formulation, and (3) the comparison of shear modulus reduction and damping curves with published data and experiments.

Table 1. PDMY parameters of Leighton Buzzard Sand (Lyon et al. 2022)

Parameter	Value
Density	1.55 ton/m^3
Reference shear modulus	143 Mpa
Reference bulk modulus	310 MPa
Friction angle	32°
Peak shear strain	0.1
Mean pressure exponent	0.5
Phase transformation angle	27°
Contraction coefficient	0.05
Dilation coeficient 1	0.6
Dilation coeficient 3	3
Initial void ratio	0.71

2.1   Stage 1: Gravity Loading

The analysis begins with the gravity loading of a continuous (unexcavated) soil deposit, in which the soil behaves elastically. This stage was performed through a dynamic analysis with large damping ratio to minimize the vertical response. Once the static equilibrium is reached, the non-linear behavior of the PDMY material is activated; then, the dynamic analysis is continued to attenuate residual oscillations in the model. The resulting profile of vertical and horizontal stresses in the soil elements is shown in Fig. 2, from which the at-rest (Ko) coefficient is approximately 0.42.
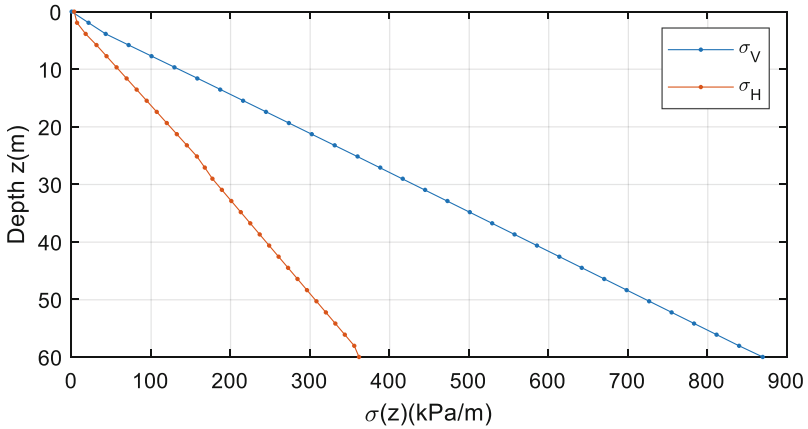
Fig. 2. Horizontal and vertical stresses in the soil deposit.

2.2 Stage 2: Excavation Sequence

After stage 1 is completed, a simplified excavation and construction sequence is modeled in four steps, as shown schematically in Fig. 3. The sequence begins with the removal of the soil elements in the top-right quadrant (see Fig. 3) followed by a static equilibrium analysis; this process simulates a staged excavation as in the SEM method, allowing to redistribute the internal forces in the soil. Then, the lining construction is modeled as elastic beam elements added on this quadrant under non-slip conditions, once again, followed by a static equilibrium analysis to dampen any oscillations.

The procedure of removing soil elements, adding the lining, and proceeding to equilibrium is repeated for the remaining quadrants in the counterclockwise direction, refer to the inset of Fig. 3, where the dashed fill denotes an "excavated" area. Finally, the stress state of the soil-lining system at the end of excavation is defined as the initial conditions for the subsequent dynamic analyses.

The settlement evolution computed on the soil right above the tunnel is shown in Fig. 3. This plot shows that most of the tunnel deformation occurs during the excavation of the first and second quadrants; also notice that the vertical oscillations at the end of each stage are damped out asymptotically as intended.
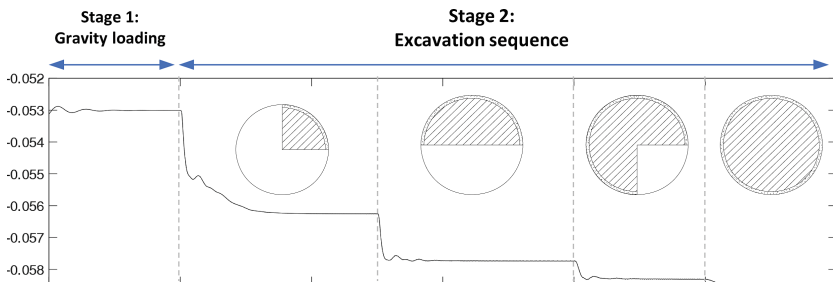

Fig. 3. Model settlements during gravity analysis and excavation

2.3   Stage 3: Dynamic Analysis

The final stage consists of simulating the seismic response of the system, for which a suite of ground motions from subduction earthquakes have been selected and scaled to two intensity levels. As mentioned above, the initial conditions for the dynamic analysis were inherited from the excavation analysis. The ground motions were input as a distributed shear load at the base and the equations of motions were solved using the Newmark integration scheme ($\gamma = 0.5$ and $\beta = 0.25$), and a constant integration step of $\Delta t = 0.005$ s.

Thirty-three (33) ground motions were selected from the SIBER-RISK database (Castro et al. 2020) and scaled at two intensity levels, consistent with return periods of 500 and 2500 years. As an example, Figs. 4, 5 and 6 show the histories of axial load, shear load, and bending moment at the top of the tunnel due to ground motions of varying intensity. Notice from Fig. 4 and 5 the large residual loads which are due to large volumetric deformations in the ground.
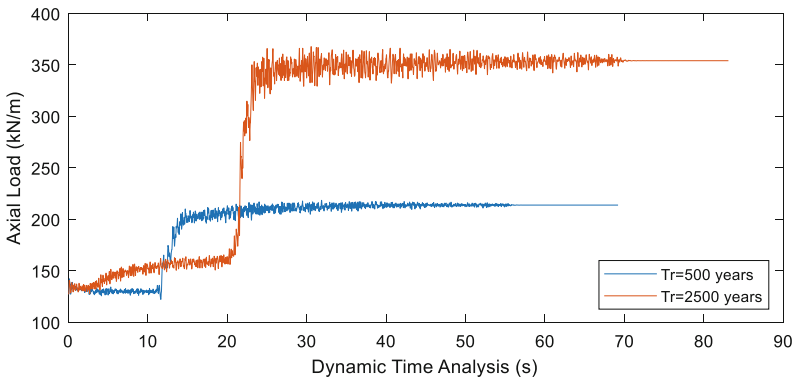

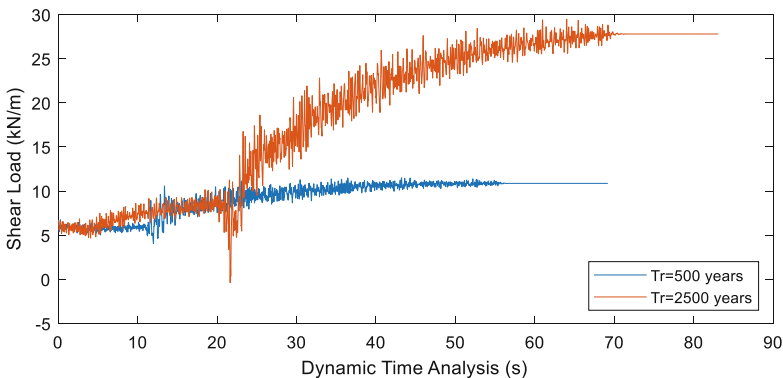**Fig. 4.** Axial load top of tunnel lining during dynamic analysis.

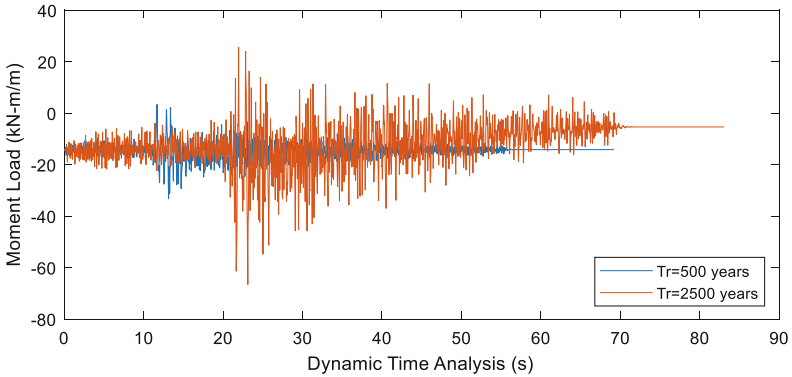**Fig. 5.** Shear load top of tunnel lining during dynamic analysis.

Fig. 6. Moment load top of tunnel lining during dynamic analysis.

Likewise, Fig. 7 shows the horizontal displacement at the free surface, reaching values up to 4 cm and 2 cm for the 2500- and 500-year ground motions, respectively.

Finally, from these results obtained in the top of the tunnel lining, the predominance of the axial load and bending moment over the shear stresses is observed for both return periods.
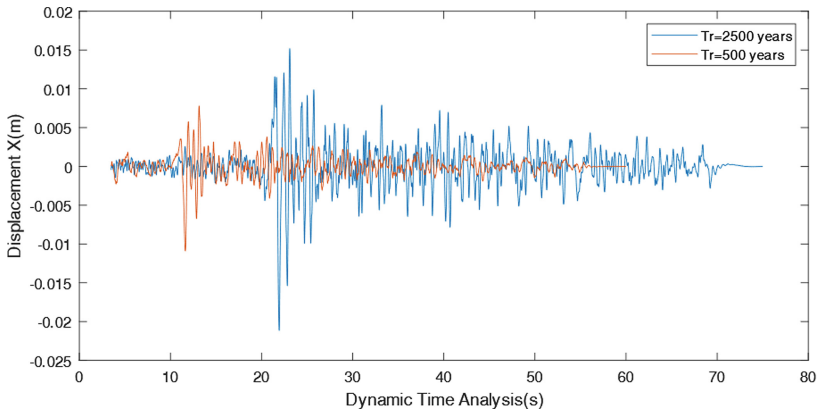

Fig. 7. Horizontal displacement in top surface during dynamic analysis (i.e., Stage 3).

3   Results

This section presents the static forces developed as a result of soil excavation and lining construction, and the static plus dynamic loads due to ground motions. From these results, history of internal forces, and deformations at different control points were obtained to address the research hypothesis.

3.1   Static Internal Forces

This section describes the lining forces developed during soil excavation and lining construction, i.e., referred herein as stage 2. The polar plots in Figs. 8, 9 and 10, show the axial load, shear loads, and bending moments, respectively, as a function of the orientation measured in degrees. The 4 color lines indicate the 4 excavation stages.

As apparent from these Figures, the maximum internal forces occur on the lining elements of the first quadrant during the final excavation stages. In the case of shear loads, a maximum value of 27.32 kN/m is reached on the beam elements located between 0 and 7.5° (Fig. 8). Likewise, peak axial loads of 150 kN/m and peak bending moments of 28 kN m/m are developed on the first quadrant at approximately 45°. Notice that the static loads on the quadrants 2, 3 and 4 are significantly lower.
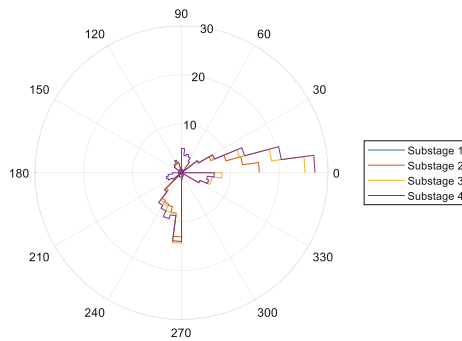

Fig. 8. Distribution of shear load (V)(kN/m) in the tunnel lining during excavation.
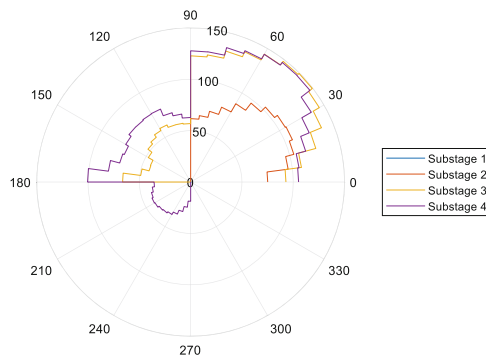

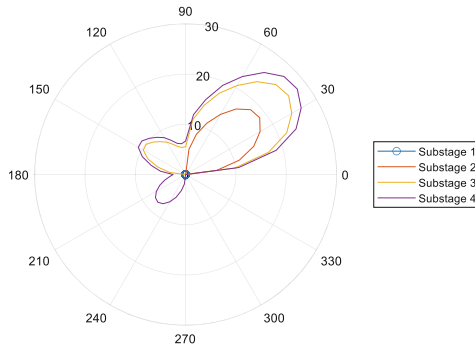**Fig. 9.** Distribution of axial load (P)(kN/m) in the tunnel lining during excavation.

Fig. 10. Distribution of moment load (M)(kN-m/m) in the tunnel lining during excavation.

3.2   Dynamic Response of Tunnel

Envelopes of lining forces are presented in Figs. 11, 12 and 13 for each ground motion subset; left plots correspond to the ground motions in the first hazard level (500-yearreturn period) and right plot correspond to the second hazard level (2500 years return period).

Notice that shear loads reach peak values of up to 35 kN/m in both hazard levels. (Fig. 11), which represent only a mild increment with respect the static loads. In contrast, that axial loads reach values of 350 kN/m in the first hazard level, and 425 kN/m in the second hazard level (Fig. 12), which in the last case, almost triples the static values. Notice that dynamic axial loads are more or less uniform around the lining.
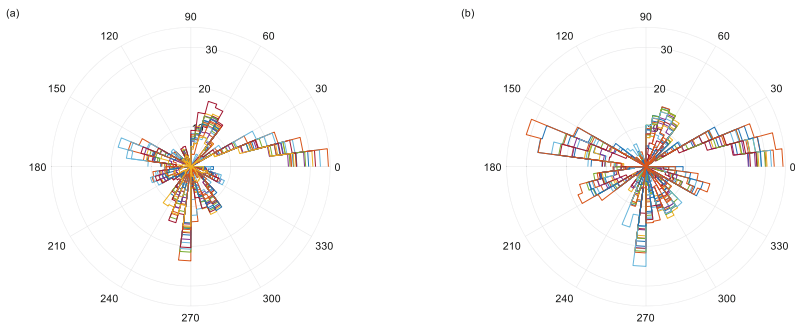

Fig. 11. Distribution of shear forces (V)(kN/m) in the lining for dynamic analyses (a) return period of 500 years, and (b) return period of 2500 years.
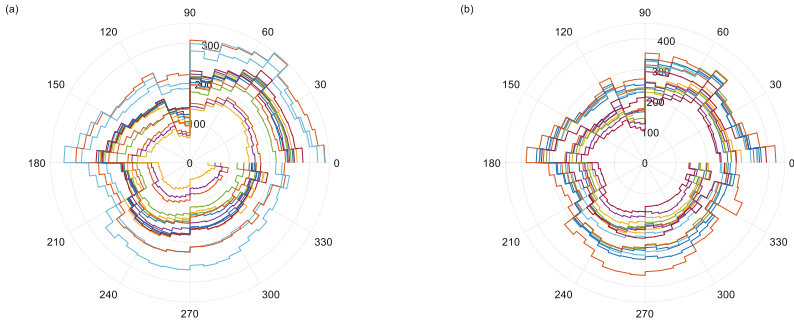
Fig. 12. Distribution of axial loads (P)(kN/m) in the lining for dynamic analyses (a) return period of 500 years, and (b) return period of 2500 years.

Envelopes of bending moment are shown in Fig. 13. Importantly, the highest bending moment demand occurs at or near the tunnel shoulders (i.e., at angles of 45°, 135° 225°, 315°), with values up to twice the static bending moments. Also, notice that the lowest bending moments occur at angles 0°, 90°, 180°, 270°.
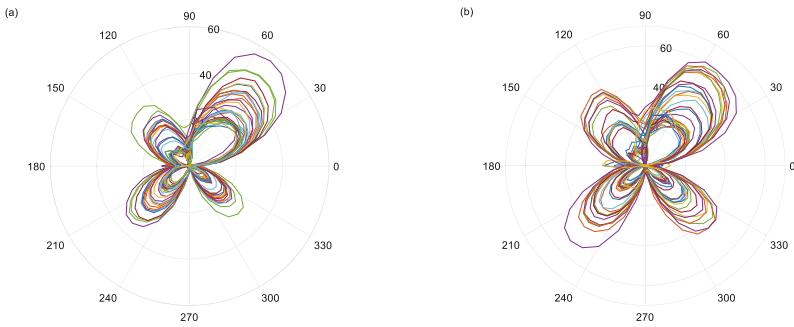

Fig. 13. Distribution of bending moments (M)(kN-m/m) in the lining for dynamic analyses (a) return period of 500 years, and (b) return period of 2500 years.

4   Lining Design

Based on the previous results, two load conditions are considered to accept or reject the working hypothesis (tunnels designed with adequate factors of safety for static loads can resist large ground motions without substantial damage). To answer this question, the lining was designed using AASTHO-LRFD recommendations (ASSHTO, 2017) along with the ACI-318 design code (ACI, 2014) considering only the static load combinations. Then, the resulting design is verified using the internal forces from the dynamic analysis from which the main conclusions can be drawn.

The lining was designed as a beam-type element subjected to axial load and bending moments following the ACI-318 (ACI 2014). The beam reinforcement is

composed of 5 steel bars (2ϕ28 and 3ϕ28) with a 5 cm cover and bar clearance greater than 1.5 inches. The gross height of the beam is 30 cm, corresponding to the typical thickness used for metro tunnel (Thomas 2009). Finally, the concrete strength is 30 MPa, and the steel reinforcement corresponds to A63-42H type bars.

The axial load – bending moment interaction diagram of Fig. 14 shows the ultimate capacity (blue line) and nominal capacity (red line) for the proposed lining design. The red marker (stars) represents the axial load and bending moment pairs from the static analysis, which fall gently within the interaction diagram, meaning that the lining behaves almost within the linear elastic range during construction.
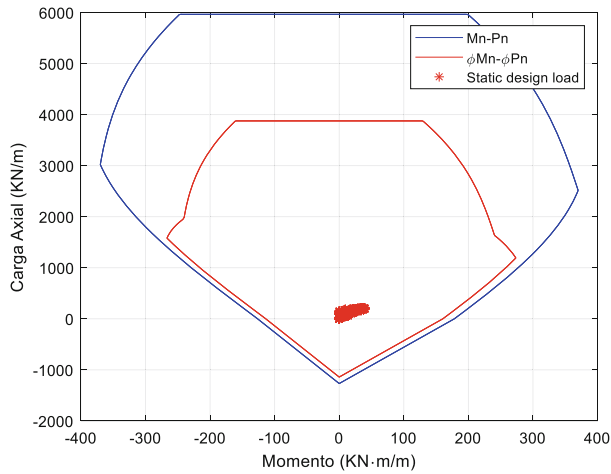

Fig. 14. P-M interaction diagram of lining designed with static load through ASSHTO-LRFD (2017).

The static design of the lining was tested with the loads results of the dynamic analysis (Stage 3) based on the dynamic load combination called Extreme Event T-I (ASSHTO 2017) the design loads are obtained for the sets of earthquakes associated with 500 and 2500 years of return period.

Figure 15 shows the axial load and bending moment envelopes from the dynamic analysis of Stage 3, considering all 33 earthquakes at each hazard level. Similar to the static loading conditions, notice that the seismic design loads fall within the nominal capacity curve with ample margins of safety.
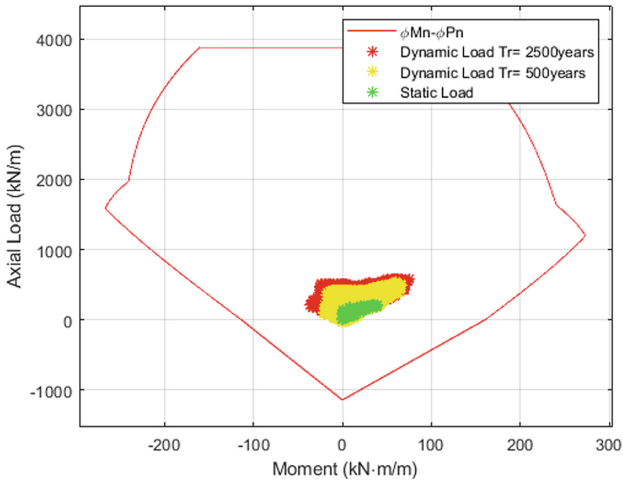
Fig. 15. P-M interaction diagram of lining designed with static and dynamic loads for 500 and 2500 years of retorn period.

5   Conclusions

In conclusion, through the lining statical design tested with the dynamic loads associated to 500 y 2500 years of return period we were able to verify our initially hypothesis raised, and it was possible for the lining designed with static loads to support dynamic loads associated to medium-several earthquakes.

The model convergence was fast and effective through pseudostatic analysis, which allowed us to build an efficient model for this type of analysis. Also, with respect to the model it was possible to conclude that the uncertainty of the ground motion is essential in the design of model and the lining.

Finally, we were also able to conclude that was most simple resolved a statical model with a pseudostatic analysis because that way we should not have changed the boundary conditions.

References

1. Kiyota, T., Ikeda, T., Konagai, K., Shiga, M.: Geotechnical damage caused by the 2016 Kumamoto earthquake, Japan. Int. J. Geoeng. Case Histor. **4**(2), 78–95 (2017)
2. McKenna, F.: OpenSees: a framework for earthquake engineering simulation. Comput. Sci. Eng. **13**(4), 58–66 (2011)

 3. Lyon, B., Candia, G., Gutiérrez, C., Macedo, J.: Performance-based analysis of Transit tunnels in the Chilean subduction zone. Soil Dyn. Earthq. Eng. **152**, 107047 (2022)
 4. Castro, S., Benavente, R., Crempien De La Carrera, J.G.F., Candia, G., Llera Martin, J.C.D. L.: Conjunto de datos: SIBER-RISK Strong Motion Database (2020)
 5. Mejia, L.H., Dawson, E.M.: Earthquake deconvolution for FLAC. In 4th International FLAC Symposium on Numerical Modeling in Geomechanics, pp. 04–10 (2006)
 6. Yang, Z., Elgamal, A.: Command Manual and User Reference for OpenSees Soil Models and Fully Coupled Element Developed at University of California at San Diego By (2003)
 7. Thomas, A.: Sprayed Concrete Lined Tunnels. Taylor & Francis, (2009)
 8. AASHTO: LRFD Road Tunnel Design and Construction Guide Specifications, First Edition (2017)
 9. ACI: Building code requirements for structural concrete (ACI 318-08) and commentary. American Concrete Institute (2008)
10. Riddell, R., Hidalgo, P.: Diseño estructural. Ediciones UC (2018)
11. Arteta, C.A., Abrahamson, N.A.: Conditional scenario spectra (CSS) for hazard-consistent analysis of engineering systems. Earthq. Spectra **35**(2), 737–757 (2019)